

Electro-osmosis of nematic liquid crystals under weak anchoring and second-order surface effects

Antarip Poddar, Jayabrata Dhar, and Suman Chakraborty*

Department of Mechanical Engineering, Indian Institute of Technology Kharagpur, Kharagpur-721302, India

(Received 27 March 2017; revised manuscript received 7 June 2017; published 24 July 2017)

Advent of nematic liquid crystal flows has attracted renewed attention in view of microfluidic transport phenomena. Among various transport processes, electro-osmosis stands as one of the efficient flow actuation mechanisms through narrow confinements. In the present study, we explore the electrically actuated flow of an ordered nematic fluid with ionic inclusions, taking into account the influences from surface-induced elasticity and electrical double layer (EDL) phenomena. Toward this, we devise the coupled flow governing equations from fundamental free-energy analysis, considering the contributions from first- and second-order elastic, dielectric, flexoelectric, charged surface polarization, ionic and entropic energies. The present study focuses on the influence of surface charge and elasticity effects in the resulting linear electro-osmosis through a slit-type microchannel whose surfaces are chemically treated to display a homeotropic-type weak anchoring state. An optical periodic stripe configuration of the nematic director has been observed, especially for higher electric fields, wherein the Ericksen number for the dynamic study is restricted to the order of unity. Contrary to the isotropic electrolytes, the EDL potential in this case was found to be dependent on the external field strength. Through a systematic investigation, we brought out the fact that the wavelength of the oscillating patterns is dictated mainly by the external field, while the amplitude depends on most of the physical variables ranging from the anchoring strength and the flexoelectric coefficients to the surface charge density and electrical double layer thickness.

DOI: [10.1103/PhysRevE.96.013114](https://doi.org/10.1103/PhysRevE.96.013114)**I. INTRODUCTION**

Electrokinetic transport phenomena of complex fluids through microconfinements have been elaborately studied in the literature [1–3] due to its various applications in biomedical engineering [4–6], energy conversion processes [7–10], environmental sciences, and thermal management of electronic packages, to name a few. Emergence of electrokinetic transport of ordered fluids, especially of anisotropic liquid crystalline medium, has led to numerous studies in recent times that explore the flow behavior and nonlinear effects under the scope of microscale dynamics [11]. Nematic Liquid Crystals (NLCs) are among such ordered fluids that display an orientational order across the study length scales [12,13]. The molecules of NLCs have, in general, rod-shaped structures and remain arranged with a typical specific order. The average molecular long-axis alignment of such NLC molecules is denoted using a unit vector \mathbf{n} , known as the director [12,13].

When confined within a microchannel, NLCs show intriguing elastic and flow response to external stimuli, which have recently motivated numerous microfluidic studies of such nematic cells [14–17]. In the context of flow actuation through narrow conduits, electro-osmosis, defined as the mechanism of actuating a fluid in contact with a charged surface by the application of an external electric field [18–21], has emerged as a promising means of energy efficient flow actuation process. Such flows are generally characterized by a charged surface due to certain physicochemical interactions [18,19], among which few of them involve mechanisms such as selective charge adsorption, photoelectric surface activation, surface ionic dissociation at the liquid-substrate interface, etc. Balance between the electrostatic and the entropic interactions among the ionic species results in a charge distribution across the

channel with a dominant counterion (ions of opposite polarity to that of the substrate) density manifested at the vicinity of the surface. The layer of immobilized counterions adjacent to the surface is referred to as the Stern layer or compact layer, while the region to which the charge density gradient is present is known as the electrical double layer (EDL). Upon application of a longitudinal electric field, movement of surplus ions within the EDL sets in due to electrostatic forces. Consequent viscous interactions between the moving ions and solvent molecules exert a body force, thus triggering a linear electro-osmotic flow [20,22]. Theoretical and experimental investigations of linear electro-osmotic flows, wherein the flow velocity depends linearly with the applied field, have been robustly studied in electrokinetic literature [18–20,22–25]. Following this, nonlinear electro-osmosis (known as induced charge electro-osmosis or ICEO) around polarizable surfaces, such as metallic colloids, has been realized where the electro-osmotic velocity varies quadratically with the applied electric field [26–28]. Very recently, Lazo and coworkers [11] experimentally demonstrated a nonlinear electro-osmotic phenomenon in nematic liquid crystals exploiting the spatial charge separation owing to the anisotropy in electrical conductivity and consequent director distortion. Subsequently, a corresponding comprehensive theory was developed by Tovkach *et al.* [29]. Although liquid crystal electro-osmosis (LCEO) serves as a significant facet in microfluidic transport, sustained flow actuation employing a DC field in the scope of linear electro-osmosis through a narrow conduit has never been studied for such complex anisotropic liquids.

A simultaneously prominent factor for NLC dynamics within a narrow confinement is the dependence of macroscopic behavior of the NLC director on the interacting solid substrates that confines it [13,14]. Owing to high surface-to-volume ratio of nematic cells, the boundary effects propagate far into the bulk nematic medium and, consequently, pose a significant influence on the equilibrium director distortion

*suman@mech.iitkgp.ernet.in

and velocity distribution [14,30–32]. In the absence of any external perturbations, the NLC director gets oriented in a certain preferential direction at the substrate-fluid interface, denoted by its easy direction. Upon application of an external field, the orientation of liquid crystal molecules at the interface may deviate from the easy direction, giving rise to a phenomenon known as “weak anchoring”. Such forms of weak surface alignment of directors have been realized in various experimental studies that include soft rubbing of a polymer film, oblique evaporation of SiO₂ [33], photoinduced ordering [34], and chemical patterning of surfaces [35,36]. Along with such experiments, parallel theories have also been developed to account for the surface-induced influence on the resulting director orientation [37]. Rapini and Papoular [38] proposed that the weak anchoring condition stems from an additional preliminary surface energy contribution to the total free energy of the nematic cell. Coupling the weak anchoring condition with the first-order elastic theory for NLC director dynamics, introduced by Frank and Oseen [13], satisfactorily captures the director field in the bulk. However, it fails to explain the rather intricate director deformation observed close to the nematic-substrate interface [39,40]. Following this, a modification to the surface energy by introducing a surface-like elasticity due to mixed splay-bend contribution (with elastic constant K_{13}) [41,42] was attempted. Nevertheless, such modification to the elastic free energy makes it unbounded from below, resulting in surface discontinuity in the director orientation [39,43,44]. This paradox has been resolved afterwards by including higher-order elasticity terms in the bulk free-energy contribution [45,46]. The sharp director variation, which is observed in an extremely thin transition region near the surface having a characteristic length scale of the order of molecular interaction, may then be successfully captured by considering a more accurate second-order elastic theory pertinent in this narrow sublayer [47–49]. In regards to the above discussion, one must account for the compounding influence of second-order elasticity with weak anchoring effects for microenvironment flows. However, recent studies of electrokinetic flows through narrow conduit have not properly addressed the aforementioned concerns.

In the present study, we, therefore, address the sustained flow actuation mechanism within a NLC parallel-channel cell employing linear electro-osmosis, taking into account second-order elasticity prominence adjacent to the bounding surface with weak anchoring condition. NLCs have been known to induce EDLs adjacent to the bounding substrate due to surface charge adsorption in the presence of ionic impurities within the NLC medium [50–55]. In the presence of such an EDL, application of an external field results in an electro-osmotic flow through the narrow conduit. It is noteworthy that, contrary to the recent works [56,57] on nonlinear electro-osmosis, where a predefined director orientation was employed neglecting the reorientation due to dielectric and viscous torques, we considered a two-way coupling between the director orientation, potential distribution, and velocity distribution. In our case, an equilibrium distortion behavior of the nematic cell results from a competition among elastic, viscous, dielectric, flexoelectric and surface polarization torques. Energies from the contribution of the ionic species distribution were also carefully taken into account to model the flow of NLC fluids.

We have further relaxed the point-charge approximation for the ionic impurities to include the excluded-volume effects of the finite hydration shell size [58]. For the nematodynamic estimation, we employ the classical Leslie-Ericksen flow model [13] governing the director deformation and fluid flow characteristics for the NLC medium. We have considered homeotropic easy-direction arrangement of the director at the boundaries. Interestingly, here we observe the formation of optical periodic stripes of the director configuration, especially at higher applied electric fields. Such observations are common for director arrangements in NLC flows with surface confinements [15,30]. The present study is dedicated to bringing out the development of a comprehensive theory and resulting implications of linear electro-osmosis of NLCs due to induced surface effects, which is in contrast to the investigations made so far. Since linear electro-osmotic flows have wide avenues of applications as mentioned above, it necessitates a focused study appealing to the underlying intricate physics involved in such fundamental electrokinetic transport mechanism for ordered nematic medium.

II. MATHEMATICAL FORMULATION

For the present study, we consider a NLC with splay and bend elastic coefficients as K_{11} and K_{33} , respectively, confined between two semi-infinite parallel walls having a separation of $2h$ as shown in the schematics (Fig. 1). The nematic liquid is associated with an intrinsic dielectric anisotropy due to its distinct parallel and perpendicular dielectric constant represented by ϵ_{\parallel} and ϵ_{\perp} , respectively, while its flexoelectric coefficient is given using e_1 and e_3 . The average direction of the nematic molecules, represented by unit director vector \mathbf{n} , is assumed to vary across the channel width (y axis) with the restriction of planar deformation (director deformations remain in the flow plane). Consequently, the unit director may be reformulated in the form $\mathbf{n} = \sin \theta(y)\mathbf{i} + \cos \theta(y)\mathbf{j}$, as shown in the above schematic, while a weak anchoring condition of the director prevails at both the walls. Weak anchoring refers to the condition wherein the director orientation at any interface is evaluated by the balance of relevant surface energies.

We consider the existence of an induced EDL at the liquid-substrate interface due to certain physicochemical interactions which impose a nonlinear distribution of the charged entities dissolved in the liquid medium having a number density n_0 in the reservoir [50,59,60]. Owing to this charge at the interface, with a surface charge density σ_w , and the ionic charge distribution in the liquid domain, a transverse nonuniform electric field $E_y(y)$ gets spontaneously induced which, besides affecting the fluid rheology and the anchoring conditions. These effects, combined together, provide the necessary body force for the flow actuation of the liquid medium. Upon the application of an external longitudinal electric field E_x , electro-osmotic flow results. Here the axial velocity field is assumed to be only a function of the transverse direction $V = u(y)\mathbf{i}$.

An interesting aspect of electronematodynamic flows with weak anchoring is the intricate interplay among the director orientation, potential distribution and flow velocity. To investigate the underlying physics, we have carefully taken into account the elastic, dielectric, flexoelectric, charged surface

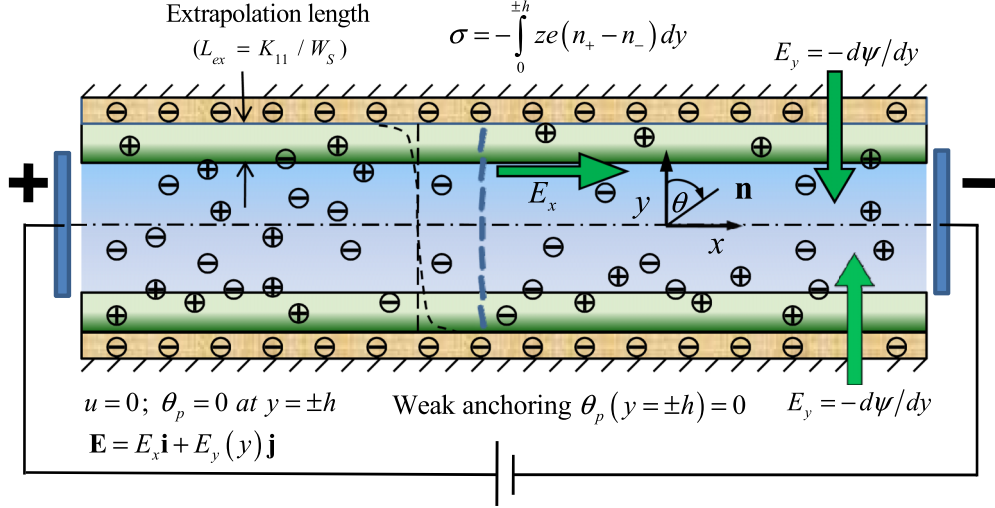


FIG. 1. Schematic representation of the electro-osmosis of an anisotropic nematic liquid crystal under the action of an external axial electric field. An electrical double layer gets induced adjacent to each of the nematic-substrate interface. Besides influencing the fluid rheology and director orientation, this provides the genesis of the flow actuation body force. A weak boundary condition with homeotropic-type easy axis is considered at both the surfaces. The extrapolar length (L_{ex}), within which the weak anchoring effects are pronounced, is also highlighted in the above schematic.

polarization, ionic, and entropic energies of the system. We have further assumed a negligible conductive anisotropy for the NLC with a consequence that the charge separation due to the Carr-Helfrich effect [61] remains absent. This assumption is consistent with numerous previous studies [62–66], which explicitly considered the ionic presence within the LC phase but neglected charge separation phenomena. This allows us to focus the present study within the domain of linear electro-osmosis. Following the aforementioned notion, we proceed to evaluate the potential distribution within the EDL and equilibrium director configuration of the nematic phase with weak anchoring conditions by considering the total free energy F that incorporates the elastic energy of the nematic molecules, the dielectric energy inherent to its anisotropic nature, the flexoelectric energy attributed to shape-induced polarization of the molecules, the internal energy, and the entropic contributions that accounts for the ionic charge distribution and their excluded volume effects.

The elastic energy associated with the director deformation in the NLC phase reads [67–70]

$$F_{\text{elast}} = \int_V f_V dV + \int_S (f_{13} + f_{24} + f_S + f_{\text{pol}}) dS, \quad (1)$$

where the integrals are taken over volume V and surface S of the nematic sample. The bulk free energy f_V due to elastic distortion of the NLC director is obtained from the first-order elasticity theory as proposed by Frank and Oseen [12,13] which takes the form

$$f_{V,1\text{st order}} = \frac{1}{2} [K_{11}(\nabla \cdot \mathbf{n})^2 + K_{22}(\mathbf{n} \cdot \nabla \times \mathbf{n})^2 + K_{33}(\mathbf{n} \times \nabla \times \mathbf{n})^2]. \quad (2)$$

To capture the sharp variation of the director field within the surface transition layer and frame a well-posed variational problem [71], we resort to the second-order elastic theory [69,72]. The general expression of second-order free energy density is rather complex, involving a set of 35 new elastic

constants. This makes it practically impossible to solve for the equilibrium director field. However, it was further found [72] that close to a threshold of small distortion amplitude, the additional term that remains significant is given by $K^*(\nabla^2 \mathbf{n})^2 \approx K^*(\frac{d^2 \theta}{dy^2})^2$, where K^* is the bulk second-order elastic constant. Thus, in this limiting case the resultant bulk free-energy density is defined by [39,43,69,72]

$$f_{V,2\text{nd order}} = \frac{1}{2} [K_{11}(\nabla \cdot \mathbf{n})^2 + K_{22}(\mathbf{n} \cdot \nabla \times \mathbf{n})^2 + K_{33}(\mathbf{n} \times \nabla \times \mathbf{n})^2] + K^*(\nabla^2 \mathbf{n})^2. \quad (3)$$

Though the consideration of a bulk second-order elastic constant is valid in the surface transition layer, it fails to track the larger distortion of directors far inside the nematic cell. Hence, we employ a two-layer model [47], where the flow domain is divided into a subsurface region spanning up to a distance δ in the vicinity of each wall and a bulk-layer covering the rest of the nematic cell. The transition layer thickness δ is considered to be of few characteristic lengths ($\sqrt{2K^*/K_{11}}$) [47]. Toward this, we employ the first- and second-order elastic theories in the bulk and surface layer, respectively. Here, f_{13} and f_{24} describe the second-order surface elastic energy terms given by $f_{13} = K_{13} \nu \cdot \mathbf{n}(\nabla \cdot \mathbf{n})$ and $f_{24} = -\frac{1}{2}(K_{22} + K_{24}) \nu \cdot [\mathbf{n}(\nabla \cdot \mathbf{n}) + \mathbf{n} \times \nabla \times \mathbf{n}]$, respectively; ν represents the unit surface normal, K_{13} denotes the mixed splay-bend elastic constant, and K_{24} denotes the saddle-bend elastic constant. Further, f_S stands for free-energy density of nematic-substrate interaction given by [38,48]

$$f_S = \frac{1}{2} W_S \sin^2(\theta - \theta_p), \quad (4)$$

where W_S and θ_p are the anchoring energy constant and the director orientation along the easy axis, also known as the pretilt angle, respectively.

Besides, the elastic energy due to director deformation, an additional energy component in the presence of an electric field F_{el} gets associated with the NLC phase having dissolved

ionic impurities. The cumulative electrical energy incorporates the energies originating from liquid dielectric anisotropy (F_{de}), gradient flexoelectric molecular nature F_{fe} , and internal energy F_{int} due to the presence of free ions as $F_{el} = F_{de} + F_{flex} + F_{int}$. The dielectric energy density may be evaluated from the classical description $F_{de} = -\frac{1}{2} \int \mathbf{D} \cdot \mathbf{E} dV$, where the electric displacement vector \mathbf{D} is defined in the case of liquid crystals as $\epsilon_0[\epsilon_{\perp} \mathbf{E} + \epsilon_a(\mathbf{E} \cdot \mathbf{n})\mathbf{n}]$, and the electric field vector is given by $\mathbf{E} = E_x \mathbf{i} + E_y(y)\mathbf{j}$. Here, $\epsilon_a = \epsilon_{\parallel} - \epsilon_{\perp}$ is known as the dielectric anisotropy, ϵ_0 is the absolute permittivity of free space, E_x denotes the applied axial field, $E_y = -\frac{d\psi}{dy}$ denotes the spontaneously induced inhomogeneous transverse field, and $\psi(y)$ represents the potential distribution within the EDL. This results in the anisotropic dielectric energy of the form

$$F_{de} = \int -\frac{\epsilon_0 \epsilon_a}{2} [E_x \sin(\theta) + E_y(y) \cos(\theta)]^2 - \frac{\epsilon_0 \epsilon_{\perp}}{2} [E_x^2 + E_y(y)^2] dy. \quad (5)$$

Mechanical deformation of the director field in NLCs gives rise to a net electric polarization analogous to the piezoelectric effect in solids. This type of macroscopic polarization induced by a bend or splay distortion, is commonly known as flexoelectric polarization [73]. The flexoelectric counterpart of the energy density for the nematic molecules is determined using $F_{flex} = -\int \mathbf{P}_{fl} \cdot \mathbf{E} dV$, where the induced polarization for such ordered nematic is given by [37,74] $\mathbf{P}_{fl} = e_1(\mathbf{n} \nabla \cdot \mathbf{n}) + e_3(\mathbf{n} \times \nabla \times \mathbf{n})$, where e_1 and e_3 are the flexoelectric coefficients. The resultant flexoelectric energy functional reads

$$F_{flex} = \int \left\{ [(e_1 \sin^2(\theta) + e_3 \cos^2(\theta))E_x + (e_1 - e_3) \times \sin(\theta) \cos(\theta)E_y(y)] \frac{d\theta}{dy} \right\} dy. \quad (6)$$

Besides the flexoelectric effect, an additional nematic-substrate interaction in the form of surface polarization gets coupled with the electric field [75–79]. Such influences arise especially adjacent to an interface where the two ends of the nematic molecules have distinctive nature, resulting in an uncompensated dipole moment parallel to the director. This surface polarization plays an important role while determining the surface torque, especially in weak anchoring condition having homeotropic-type easy axis [75]. The associated energy density of the surface polarization is given by [75]

$$f_{pol} = -m_p(\vec{n} \cdot \vec{E}) = -m_p(E_x \sin(\theta) + E_y \cos(\theta)), \quad (7)$$

where m_p stands for the surface dipole density.

The contribution to the internal energy is from the dissolved ionic species within the nematic sample, which comprises the ionic electrostatic energy having the form [80]

$$F_{int} = \int z e \phi(x, y)(n_+ - n_-) dV, \quad (8)$$

where the associated total potential due to the combined applied and induced electric field reads $\phi(x, y) = \psi(y) + (\phi_0 - x E_1)$.

It must be appreciated that the dissolved ions usually have finite-size effects that should be taken into consideration,

which restricts excessive ionic crowding near the wall, particularly for situations involving high ionic concentration and strong electrostatic interactions. Relaxing the point-charge approximation, the entropic contribution considering the finite ionic shell size is given by the form [81,82]

$$F_{entropic} = -TS = k_B T \int dy [n_+ \ln(a_+^3 n_+) + n_- \ln(a_-^3 n_-) - n_+ - n_-] + \frac{k_B T}{a^3} \int dy [(1 - a_+^3 n_+ - a_-^3 n_-) \times \ln(1 - a_+^3 n_+ - a_-^3 n_-)]. \quad (9)$$

The above formulation allows the inclusion of excluded volume effects within the continuum modeling of the ionic distribution where the number density of positive (negative) ions is given by $n_+(n_-)$, while their corresponding ionic shell size is denoted using $a_+(a_-)$. Further for the sake of simplicity, we assume $a = a_+ = a_-$. From the individual energy contributions, the cumulative energy density for the nematic phase finally reads

$$F = \frac{1}{2} \rho v_i v_i + F_{elast} + (F_{de} + F_{flex} + F_{int}) + F_{entropic}. \quad (10)$$

Following the free-energy form, we now proceed to minimize it with respect to the electrostatic potential as $\frac{\delta F}{\delta \psi} = 0$ that results in equation governing the distribution of potential and the ionic species within the liquid phase at equilibrium condition. The modified Poisson-type equation, which couples the ionic and the potential distribution with director configuration, reads

$$\epsilon_0(\epsilon_a \cos^2(\theta) + \epsilon_{\perp}) \frac{d^2 \psi}{dy^2} - \epsilon_0 \epsilon_a \left(E_x \cos(2\theta) + \sin(2\theta) \frac{d\psi}{dy} \right) \frac{d\theta}{dy} + \frac{1}{2} (e_1 - e_3) \sin(2\theta) \frac{d^2 \theta}{dy^2} + (e_1 - e_3) \cos(2\theta) \left(\frac{d\theta}{dy} \right)^2 + z e (n_+ - n_-) = 0. \quad (11)$$

The corresponding electrochemical potential for the present system, which may be obtained as $\mu_{\pm} = \frac{\delta F}{\delta n_{\pm}}$ [80], is a gradient-free quantity for equilibrium condition leading to the modified Boltzmann distribution as [83,84]

$$n_{\pm} = \frac{n_0 \exp(\mp e z \psi / k_B T)}{1 + v(\cosh(e z \psi / k_B T) - 1)}. \quad (12)$$

In the above form, $v = 2n_0 a^3$ denotes the steric factor and n_0 is the number density of ions in the bulk reservoir. Substituting the Boltzmann distribution n_{\pm} into Poisson equation, the modified Poisson-Boltzmann equation for the NLC phase is obtained. The cumulative charge within half the channel is equal and opposite to the charge density induced at the wall, which provides us with the necessary boundary condition applicable to either of the walls. Consequently, the condition at the upper boundary reads

$$\sigma_w(y=1) = -\int_0^h \rho_e dy = \int_0^h \frac{2ze n_{\infty} \sinh(ez\psi/k_B T)}{1 + v(\cosh(ez\psi/k_B T) - 1)} dy, \quad (13)$$

where $\rho_e = e \sum_i z_i n_i = ez(n_+ - n_-)$ represents the net charge density. In a similar manner, the boundary condition for the lower plate can be derived.

To obtain the governing equation for the angular momentum balance of the director, we resort to the principle of minimum energy dissipation as followed by Tovkach *et al.* [29]. The governing form valid within each of the two thin-surface sublayers, i.e., $-h \leq y \leq -(h - \delta)$ and $(h - \delta) \leq y \leq h$, reads

$$\begin{aligned} & 2K^* \frac{d^4\theta}{dy^4} - (K_1 \sin^2(\theta) + K_3 \cos^2(\theta)) \frac{d^2\theta}{dy^2} - (K_1 - K_3) \\ & \times \sin(\theta) \cos(\theta) \left(\frac{d\theta}{dy} \right)^2 - (\alpha_3 \sin^2(\theta) - \alpha_2 \cos^2(\theta)) \frac{du}{dy} \\ & - \varepsilon_0 \varepsilon_a \left\{ \frac{1}{2} \sin(2\theta) \left[E_x^2 - \left(\frac{d\psi}{dy} \right)^2 \right] - E_x \frac{d\psi}{dy} \cos(2\theta) \right\} \\ & + \frac{1}{2} (e_1 - e_3) \sin(2\theta) \frac{d^2\psi}{dy^2} = 0, \end{aligned} \quad (14)$$

while the form governing the bulk director dynamics, i.e., $-(h - \delta) \leq y \leq (h - \delta)$, is given by

$$\begin{aligned} & (K_1 \sin^2(\theta) + K_3 \cos^2(\theta)) \frac{d^2\theta}{dy^2} + (K_1 - K_3) \sin(\theta) \cos(\theta) \\ & \times \left(\frac{d\theta}{dy} \right)^2 + (\alpha_3 \sin^2(\theta) - \alpha_2 \cos^2(\theta)) \frac{du}{dy} \\ & + \varepsilon_0 \varepsilon_a \left\{ \frac{1}{2} \sin(2\theta) \left[E_x^2 - \left(\frac{d\psi}{dy} \right)^2 \right] - E_x \frac{d\psi}{dy} \cos(2\theta) \right\} \\ & - \frac{1}{2} (e_1 - e_3) \sin(2\theta) \frac{d^2\psi}{dy^2} = 0, \end{aligned} \quad (15)$$

where α_i ($i = 1$ to 6) are the Leslie viscosities. Here we have considered the definitions of the director \mathbf{n} and velocity \mathbf{V} as given above.

The boundary conditions, as found by employing the variation of the total energy [Eq. (10)] at the boundary surface, yields four nonlinear conditions that reads

$$K^* \theta'' - K_{13} \sin(2\theta) = 0 \quad \text{at } y = -h, \quad (16)$$

$$K^* \theta'' - K_{13} \sin(2\theta) = 0 \quad \text{at } y = h, \quad (17)$$

$$\begin{aligned} & K^* \theta''' - (K_{11} \sin^2(\theta) + K_{33} \cos^2(\theta) - K_{13} \cos(2\theta)) \theta' \\ & - (e_1 \sin^2(\theta) + e_3 \cos^2(\theta)) E_x - \frac{1}{2} (e_1 - e_3) \sin(2\theta) E_2 \\ & + \frac{W_S}{2} \sin(2(\theta - \theta_{p1})) + m_p (E_x \cos(\theta) - E_y \sin(\theta)) = 0 \\ & \text{at } y = -h, \end{aligned} \quad (18)$$

and

$$\begin{aligned} & K^* \theta''' - (K_{11} \sin^2(\theta) + K_{33} \cos^2(\theta) - 2K_{13} \cos(2\theta)) \theta' \\ & - (e_1 \sin^2(\theta) + e_3 \cos^2(\theta)) E_x - \frac{1}{2} (e_1 - e_3) \sin(2\theta) E_y \\ & - \frac{W_S}{2} \sin(2(\theta - \theta_{p2})) + m_p (E_x \cos(\theta) - E_y \sin(\theta)) = 0 \\ & \text{at } y = h. \end{aligned} \quad (19)$$

Here, we have assumed that the surfaces are identical and the surface polarization moments are equal and opposite in direction, i.e., $m_{pU} = -m_{pL} = m_p$ [75]. The two regions of solution are coupled by the matching conditions at the interface given as

$$\theta[at - (h - \delta)^-] = \theta[at - (h - \delta)^+], \quad (20a)$$

$$\frac{d\theta}{dy}[at - (h - \delta)^-] = \frac{d\theta}{dy}[at - (h - \delta)^+], \quad (20b)$$

$$\theta[at(h - \delta)^-] = \theta[at(h - \delta)^+], \quad (20c)$$

$$\frac{d\theta}{dy}[at(h - \delta)^-] = \frac{d\theta}{dy}[at(h - \delta)^+]. \quad (20d)$$

The sequence of equations for the potential distribution and director orientation must be closed by the balance of linear momentum governing the fluid flow velocity to determine the electro-osmotic flow conditions for a nematic LC. Toward this, we employ the Leslie-Ericksen theory for the flow of a nematic fluid with a proposed constitutive deviatoric stress relation as [12,13]

$$\begin{aligned} \sigma_{ij} = & \alpha_1 n_i n_j A_{kp} n_k n_p + \alpha_2 n_j N_i + \alpha_3 n_i N_j + \alpha_4 A_{ij} \\ & + \alpha_5 n_j A_{ik} n_k + \alpha_6 n_i A_{jk} n_k, \end{aligned} \quad (21)$$

where $N_i = Dn_i/Dt - W_{ij} n_j$ is the corotational vector representing the rate of change of director with respect to the background fluid while A_{ij} and W_{ij} is the symmetric and anti-symmetric part of the strain tensor $\nabla \mathbf{V}$. For the present study, an electro-osmotic body force density f_{eo} gets induced, where $f_{eo} = -(c_+ \nabla \mu_+ + c_- \nabla \mu_-)$, which actuates the flow through the narrow conduit. Under the above considerations and simultaneously employing the incompressibility condition of the flow ($\nabla \cdot \mathbf{V} = 0$), the governing equation for the steady, electro-osmotically driven flow of a nematic fluid through a narrow, confined cell reduces to

$$\frac{d}{dy} \left(\eta(\theta) \frac{du}{dy} \right) = -\rho_e E_x. \quad (22)$$

Here the classical no-slip boundary condition is imposed at both the walls ($\bar{u}(\bar{y} = -1) = \bar{u}(\bar{y} = 1) = 0$), while $\rho_e E_x$ gives the electro-osmotic body force density. The position-dependent apparent nematic viscosity is a function of the director alignment, which reads $\eta(\theta) = \eta_1 \sin^2\theta + \eta_2 \cos^2\theta + \eta_{12} \sin^2\theta \cos^2\theta$, where the viscosity parameters η_1, η_2 , and η_{12} are known as the Miesowicz viscosities, which, in turn, is related to the Leslie viscosities by the following relations: $\eta_1 = \frac{\alpha_3 + \alpha_4 + \alpha_6}{2}$, $\eta_2 = \frac{-\alpha_2 + \alpha_4 + \alpha_5}{2}$ and $\eta_{12} = \alpha_1$ [13]. The present physical problem is described by a set of coupled differential equations [Eqs. (11), (14), (15), and (22)] along with nonlinear interface conditions. These governing relations for the physical problem are analytically intractable, and hence, we resort to numerical methods to solve the differential equations. For this purpose, we have used the commercial finite element method package of COMSOL Multiphysics to solve the coupled nonlinear governing equations and boundary equations. Before proceeding to solve the electro-osmotic flow of the nematic crystals, we proceed to derive a dimensionless set for the above governing equations and the corresponding nonlinear boundary conditions, resulting in a more general representation of the flow characteristics.

Next, we proceed to adopt a suitable nondimensionalization scheme, to obtain the dimensionless forms of the governing equations and boundary conditions, as follows: $\bar{y} = y/h$, $\bar{\psi} = ze\psi/k_B T$, $\bar{u} = u/u_{\text{ref}}$, $\bar{E}_x = E_x/E_{x,\text{ref}}$, and $\bar{E}_y = E_y/E_{y,\text{ref}}$. Applying the small deformation limit ($\theta \rightarrow 0$), we linearize the governing equations within the surface sublayer and the corresponding boundary conditions while the governing equations beyond this region are solved in their usual forms [47]. Under these considerations, the set of equations gets reduced to the following forms.

A. Dimensionless modified Poisson-Boltzmann equation

The dimensionless form for Eq. (12) for the thin, near-surface region and the bulk is given as within the surface transition layer i.e. $-h \leq y \leq -(h - \delta)$ and $(h - \delta) \leq y \leq h$

$$\left(1 + \frac{\varepsilon_a}{\varepsilon_\perp}\right) \frac{d^2 \bar{\psi}}{d\bar{y}^2} - \frac{\bar{E}_x}{p_1} \frac{d\theta}{d\bar{y}} - \frac{\sinh(\bar{\psi})}{(1 + \nu(\cosh(\bar{\psi}) - 1))\bar{\lambda}^2} = 0, \quad (23a)$$

and in the bulk region i.e. $-(h - \delta) \leq y \leq (h - \delta)$

$$\left(1 + \frac{\varepsilon_a}{\varepsilon_\perp} \cos^2(\theta)\right) \frac{d^2 \bar{\psi}}{d\bar{y}^2} - \left(\frac{\bar{E}_x \cos(2\theta)}{p_1} + \sin(2\theta) \frac{d\bar{\psi}}{d\bar{y}}\right) \frac{d\theta}{d\bar{y}} + A_4 \left[\sin(2\theta) \frac{d^2 \theta}{d\bar{y}^2} + 2 \cos(2\theta) \left(\frac{d\theta}{d\bar{y}}\right)^2 \right] - \frac{\sinh(\bar{\psi})}{[1 + \nu(\cosh(\bar{\psi}) - 1)]\bar{\lambda}^2} = 0, \quad (23b)$$

$$\bar{\sigma}_w = \int_0^1 \frac{\sinh(\bar{\psi})}{[1 + \nu(\cosh(\bar{\psi}) - 1)]\bar{\lambda}^2} d\bar{y}. \quad (24)$$

The matching conditions read

$$\bar{\psi}[at - (1 - \delta)^-] = \bar{\psi}[at - (1 - \delta)^+], \quad (25a)$$

$$\left(1 + \frac{\varepsilon_a}{\varepsilon_\perp}\right) \frac{d\bar{\psi}}{d\bar{y}}[at - (1 - \delta)^-] = \left(1 + \frac{\varepsilon_a}{\varepsilon_\perp} \cos^2(\theta)\right) \frac{d\bar{\psi}}{d\bar{y}} \times [at - (1 - \delta)^+], \quad (25b)$$

$$\bar{\psi}[at(1 - \delta)^-] = \bar{\psi}[at(1 - \delta)^+], \quad (25c)$$

$$\left(1 + \frac{\varepsilon_a}{\varepsilon_\perp}\right) \frac{d\bar{\psi}}{d\bar{y}}[at(1 - \delta)^-] = \left(1 + \frac{\varepsilon_a}{\varepsilon_\perp} \cos^2(\theta)\right) \frac{d\bar{\psi}}{d\bar{y}} \times [at(1 - \delta)^+]. \quad (25d)$$

Here, $E_{x,\text{ref}}$ scale is considered in the order of *Fredericksz transition field* $E_{c,x}$, which is defined as the threshold electric

field above which deformations in the nematic director is observed [13,85], while $p_1 = \frac{k_B T}{E_{x,\text{ref}} h z e}$ and $A_4 = \frac{ze(e_1 - e_3)}{2(\varepsilon_0 \varepsilon_\perp) k_B T}$. Also, $\bar{\sigma}_w = \frac{ze h \sigma}{\varepsilon_0 \varepsilon_\perp k_B T}$ denotes the dimensionless surface charge density and $\bar{\lambda} = \frac{\lambda}{h} = \sqrt{\frac{\varepsilon_0 \varepsilon_\perp k_B T}{2z^2 e^2 n_0 h^2}}$; λ being the dimensional Debye screening length. It is to be noted that here the linearization is done only with respect to orientation angle θ , but the frequently used Debye–Hückel linearization [18], which is valid for small electrostatic potential range, is not employed. Thus, in terms of electrostatic potential ψ , the results of the present study will be comprehensive and general.

B. Dimensionless form of angular momentum balance equation

The corresponding dimensionless form for the linearized Eq. (14) and the bulk Eq. (15) governing the angular momentum of the NLC phase read within the surface transition layer i.e. $-1 \leq \bar{y} \leq -(1 - \delta)$ and $(1 - \delta) \leq \bar{y} \leq 1$

$$b^2 \frac{d^4 \theta}{d\bar{y}^4} - \kappa \frac{d^2 \theta}{d\bar{y}^2} + m \bar{\alpha}_2 \frac{d\bar{u}}{d\bar{y}} - q [(\bar{E}_x^2 - p^2 \cdot \bar{E}_y^2) 2\theta + 2 \cdot p \cdot \bar{E}_x \cdot \bar{E}_y] - 2w \cdot \theta \frac{d\bar{E}_y(\bar{y})}{d\bar{y}} = 0, \quad (26a)$$

and in the bulk region i.e. $-(1 - \delta) \leq y \leq (1 - \delta)$

$$(\sin^2(\theta) + \kappa \cos^2(\theta)) \frac{d^2 \theta}{d\bar{y}^2} + (1 - \kappa) \sin(\theta) \cos(\theta) \left(\frac{d\theta}{d\bar{y}}\right)^2 + m(\bar{\alpha}_3 \sin^2(\theta) - \bar{\alpha}_2 \cos^2(\theta)) \frac{d\bar{u}}{d\bar{y}} + q [(\bar{E}_x^2 - p^2 \cdot \bar{E}_y^2) \sin(2\theta) + 2 \cdot p \cdot \bar{E}_x \cdot \bar{E}_y \cos(2\theta)] + w \cdot \sin(2\theta) \frac{d\bar{E}_y(\bar{y})}{d\bar{y}} = 0. \quad (26b)$$

The various dimensionless parameters introduced in the above equation are defined as $\kappa = K_{33}/K_{11}$, $\bar{\alpha}_3 = \alpha_3/\eta_{\text{ref}}$, $E_{y,\text{ref}} = \frac{E_y}{\sigma_w/\varepsilon_0 \bar{\varepsilon}}$, $\bar{\alpha}_2 = \alpha_2/\eta_{\text{ref}}$, $q = \frac{\varepsilon_0 \varepsilon_a E_{x,\text{ref}}^2 h^2}{2K_{11}}$, $m = \frac{u_{\text{ref}} h \eta_{\text{ref}}}{K_{11}}$, $p = \frac{(k_B T/ze)}{h E_{x,\text{ref}}} \left(\frac{\varepsilon_\perp}{\bar{\varepsilon}}\right) \bar{\sigma}_w$, and $w = \frac{k_B T(e_1 - e_3)}{2ze K_{11}} \left(\frac{\varepsilon_\perp}{\bar{\varepsilon}}\right) \bar{\sigma}_w$, with $\bar{\varepsilon}$ being the average dielectric constant defined as $\bar{\varepsilon} = (\varepsilon_\parallel + 2\varepsilon_\perp)/3$. Here, b is a dimensionless characteristic interaction length, defined as $b = \frac{1}{h} \sqrt{\frac{2K^*}{K_{11}}}$. The reference viscosity has been chosen as $\eta_{\text{ref}} = \alpha_4/2$, which is the Newtonian counterpart of the NLC viscosity, as can be deduced from the deviatoric stress equation [Eq. (21)]. The velocity reference u_{ref} will be derived from the dimensional analysis of the linear momentum balance equation.

The corresponding boundary conditions Eqs. (16)–(19) take the form

$$\begin{aligned} b^2 \theta'' - (K_{13}/K_{11}) \theta &= 0, & \text{at } \bar{y} &= -1, \\ b^2 \theta'' - (K_{13}/K_{11}) \theta &= 0, & \text{at } \bar{y} &= 1, \\ b^2 \theta''' - \frac{(K_{33} - K_{13})}{K_{11}} \theta' - \frac{E_{x,\text{ref}} h (e_3 - m p)}{K_{11}} - 2w \bar{E}_y \theta + 2\bar{\gamma}(\theta - \theta_{p1}) &= 0, & \text{at } \bar{y} &= -1, \\ b^2 \theta''' - \frac{(K_{33} - K_{13})}{K_{11}} \theta' - \frac{E_{x,\text{ref}} h (e_3 - m p)}{K_{11}} - 2w \cdot \bar{E}_y \theta - 2\bar{\gamma}(\theta - \theta_{p2}) &= 0, & \text{at } \bar{y} &= 1. \end{aligned} \quad (27)$$

TABLE I. Details the symbols, magnitudes, and units of the 5CB nematic properties used for the present study.

Property	Property Value	Unit	Property	Property Value	Unit
Splay elastic constant	$K_{11} = 6.2$	pN	Leslie viscosity coefficients [13]	$\alpha_1 = -0.0060$	Pa-s
Bend elastic constant	$K_{33} = 8.2$	pN		$\alpha_2 = -0.0812$	
Dielectric permittivity (relative)	$\epsilon_{\parallel} = 18.5$ and $\epsilon_{\perp} = 7$	—		$\alpha_3 = -0.0036$	
Flexoelectric coefficients [86]	$e_1 = -25$ and $e_3 = -8.5$	pC/m		$\alpha_4 = 0.0652$	
				$\alpha_5 = 0.0640$	
				$\alpha_6 = -0.0208$	

C. Dimensionless form of linear momentum balance equation

Corresponding to the linear momentum balance Eq. (22) for the NLC fluid, we obtain its dimensionless form employing the aforementioned dimensional parameters that reads

$$\frac{d}{d\bar{y}} \left(\bar{\eta}(\theta) \frac{d\bar{u}}{d\bar{y}} \right) = \sinh(\bar{\psi}) \bar{E}_x, \quad (28)$$

where the dimensionless viscosity function for the two regions are given as within the surface transition layer i.e. $-1 \leq \bar{y} \leq -(1 - \delta)$ and $(1 - \delta) \leq \bar{y} \leq 1$:

$$\bar{\eta}(\theta) = \frac{\eta(\theta)}{\eta_{\text{ref}}} = (\eta_2/\eta_{\text{ref}}), \quad (29a)$$

and in the bulk region i.e. $-(1 - \delta) \leq y \leq (1 - \delta)$:

$$\bar{\eta}(\theta) = \frac{\eta(\theta)}{\eta_{\text{ref}}} = \sin^2\theta + (\eta_2/\eta_{\text{ref}})\cos^2\theta + (\eta_{12}/\eta_{\text{ref}})\sin^2\theta\cos^2\theta. \quad (29b)$$

Along with the no-slip boundary conditions $[\bar{u}(\bar{y} = -1) = \bar{u}(\bar{y} = 1) = 0]$, the following matching conditions are used while solving Eq. (28):

$$\bar{u}[at - (1 - \delta)^-] = \bar{u}[at - (1 - \delta)^+], \quad (30a)$$

$$\bar{\eta}_2 \frac{d\bar{u}}{d\bar{y}}[at - (1 - \delta)^-] = \bar{\eta}(\theta) \frac{d\bar{u}}{d\bar{y}}[at - (1 - \delta)^+], \quad (30b)$$

$$\bar{u}[at(1 - \delta)^-] = \bar{u}[at(1 - \delta)^+], \quad (30c)$$

$$\bar{\eta}_2 \frac{d\bar{u}}{d\bar{y}}[at(1 - \delta)^-] = \bar{\eta}(\theta) \frac{d\bar{u}}{d\bar{y}}[at(1 - \delta)^+]. \quad (30d)$$

A closer look at Eq. (29a) reveals that only one Miesowicz viscosity (η_2) survives at the subsurface region. Now the physical interpretation of the second principal Miesowicz viscosity is described as a measurable viscosity coefficient associated with the condition when director (\mathbf{n}) is parallel to the velocity gradient ($\nabla\mathbf{V}$) [13]. Since we have assumed small deformation, the director alignment in this region is almost homeotropic, i.e., along the y direction. Thus, in this limiting condition, $\mathbf{n} \parallel \nabla\mathbf{V}$ is satisfied, and hence, the appearance of η_2 alone is justified. The velocity scale $u_{\text{ref}} = \frac{2ze\epsilon_0 E_x \text{ref} h^2}{\eta_{\text{ref}}}$ is used while reaching at the dimensionless Eq. (28).

Owing to the linearized form of the governing equations very close to the boundary, we restrict our solutions to the case where the tilt angle of the director at the boundary θ_s remains close to the pretilt angle θ_p . It must be noted that the highly nonlinear set of governing equations couples the flow velocity and the director configuration with the potential distribution, a

fact that is explicitly absent in the case of electro-osmotic flows of Newtonian fluids. In what follows, we consider a homeotropic alignment with pretilt angle equal to zero and obtain the director configuration, potential distribution, and velocity profile for the NLC electro-osmotic flow. An intriguing aspect we further put forward in this study is the director tilt at the boundary, which depends nonlinearly on the surface contributions and second-order elastic energies.

III. RESULTS AND DISCUSSIONS

In this section, we demonstrate the variation of the elastic and electrostatic surface energies on the director orientation and flow characteristics for an electro-osmotic flow within the NLC cell. For a representative case, we have selected the nematic 5CB (4-Cyano-4'-pentylbiphenyl) for our calculation whose properties are detailed in Table I. In this context, Kočevar and Muševič [54] reported instances of spontaneous charging of glass surfaces while immersed in cyanobiphenil liquid crystals (5CB and 8CB). To ensure homeotropic alignment along the surface, they utilized a deposition of a monolayer of N, N-dimethyl-N octadecyl-3 aminopropyltrimethoxysilyl chloride (DMOAP). Shah and Abbot [52] also observed formation of EDLs along the interface between a liquid crystal 5CB and a model surface prepared by the self-assembly of sodium carboxylate salts on semitransparent films of gold. They came to a conclusion that partial dissociation of sodium ions from such salts promotes the formation of EDL in the LC medium. In a simultaneous investigation, Espinoza *et al.* [55] reported the orientational behavior of 5CB on differently charged surfaces and predicted the formation of EDL on the interface. In line with the above experimental observations, we have considered that a selective adsorption of negative charges is taking place at the limiting surfaces. The controllable dimensionless parameters in the present study are chosen carefully keeping in view of the corresponding practical range of the dimensional parameters involved. The induced surface charge density is varied between 10^{-4} and 10^{-2} Cm $^{-2}$ while a bulk concentration of ionic impurities is considered in order of 10^{-3} mM [54,59,86]. These result in a dimensionless Debye screening length range of $10^{-2} - 10^{-1}$ and the dimensionless surface charge density in the range of $\bar{\sigma}_w \sim 10^1 - 10^3$ if the channel half thickness is varied as $h \sim 1 - 10 \mu\text{m}$. The characteristic length $\sqrt{2K^*/K_{11}}$ varies in the order of molecular interaction (typically 20 Å) [39,47,87] giving rise to a dimensionless characteristic interaction length ($b = \frac{1}{h} \sqrt{\frac{2K^*}{K_{11}}}$) in the range of $10^{-3} - 10^{-2}$. The surface anchoring energy parameter

$\bar{\gamma} = \frac{W_S h}{2K_{11}}$ and the easy axis direction θ_p not only depends on the substrate with which it is covered but also on the surface alignment technique. In the present study, we consider the easy direction perpendicular to the substrate ($\theta_p = 0$), i.e., the homeotropic alignment. In practical applications, this situation is often realized with surface alignment techniques like stacking of amphiphilic molecules, oblique evaporation of SiO [88], deposition of monolayer lipid membrane on SiO₂ substrates [34], or topographical patterning of polymer films [89]. Moreover, owing to the positive dielectric anisotropy of such LCs, spontaneous homeotropic orientation can be achieved by virtue of a direct coupling between the surface electric field directed normal to the charged surfaces and director [52,54,55]. Following several experimental observations, it is found that W_S remains in the range of 10^{-6} to 5×10^{-5} J/m² [30,33,90]. Thereafter, using aforementioned values of h and K_{11} , the range of dimensionless anchoring energy parameter $\bar{\gamma} = \frac{W_S h}{2K_{11}}$ can be obtained as $\bar{\gamma} \sim 0.01 - 5$. The mixed splay-bend elastic constant relates to the splay elastic constant as $K_{13} = -0.2K_{11}$, which is experimentally observed by Lavrentovich and Pergamenschik [30]. In the absence of exact experimental data on the relation between surface transition layer thickness δ and the characteristic length b , the dimensionless thickness $\bar{\delta}$ will be considered to be twice the characteristic length b . Since we will consider the parametric variation of b in the following results, the variation of $\bar{\delta}$ will also get inherently incorporated. Consequently, despite the transition layer being kept fixed for numerical calculations, parametric variation of b makes our results comprehensive in this aspect. The calculated extrapolation length ($L_{ex} = K_{11}/W_S$) for the present choice of parameters lie within the range of $0.12 - 6 \mu\text{m}$, while the Debye screening length is in between ≈ 0.01 and $1 \mu\text{m}$. As a consequence, screening of flexoelectric charges by the free ions dissolved in the material is not possible. Thus, incorporation of flexoelectric effect was appropriate for the present study. Experimental observations by Nazarenko *et al.* [77] confirm the prominent existence of ferroelectric layer of molecules in the case of a nematic cell filled with 5CB with essentially homeotropic surface anchoring condition. By using both organic and inorganic alignment layers, they have found that the surface polarization can be as high as $|m_p| \sim 10^{-10} - 10^{-11}$ C/m. In this section, we sort for the influence of the surface effects from $b, \bar{\gamma}, m_p, \bar{E}_x, \bar{\lambda},$ and $\bar{\sigma}_w$ on the resulting charge distribution, director orientation, and the nature of the electro-osmotic flow velocity. Unless otherwise mentioned, the base values of these parameters are chosen as $\bar{b} = 0.01, \bar{\gamma} = 1, \bar{E}_x = 2, \bar{\lambda} = 0.1,$ and $\bar{\sigma}_w = -2000$.

Flows of NLC fluids may be characterized by topological defects, which result in singularity of director definition [12,13]. The existence of topological defects in NLC flows greatly depends on the channel dimensions and flow rates [91]. A dimensionless quantity, namely the Ericksen number ($Er = \frac{\eta_c u_c L_c}{K_c}$), is often defined in this context. For the present case, the characteristic viscosity (η_c) and the characteristic elastic constant (K_c) can be taken as $\eta_c = (\eta_1 + \eta_2)/2$ and $K_c = (K_{11} + K_{22} + K_{33})/3$, respectively [92], while the characteristic velocity is the average flow velocity (u_{av}) and characteristic length (L_c) is the channel half height (h). Both experimental [14,91] as well as theoretical studies [93–95]

exist in literature, which shows that the topological defects become significant when the Er is very high. On the other hand, we find that the actual maximum value of Er for the present problem falls within the order of ~ 10 ; although in most of the cases it remains well below or around unity. Thus, for the present set of parameters considered, we can safely consider the flow to be “elastically” laminar with the absence of topological defects and the present formulation, following the LE formalism, remains valid.

One central aspect of the present study is to observe the director distortion behavior, potential profile, and velocity distribution in the presence of the flexoelectric effect. A great amount of mismatch between the proposed values of the flexoelectric coefficients of 5CB has been observed in numerous theoretical (e.g., statistical-mechanical approach [96]) as well as experimental measurements (e.g., pyroelectric technique [97]). Hence, we have chosen a fixed value of flexoelectric coefficients according to Zakharov and Dong [96] and refrained ourselves from varying the values as a part of the parametric studies. Instead, we streamline our study to see the additional influence due to accounting of flexoelectric polarization compared to the case when it is absent.

Figure 2 depicts the variation of the surface director orientation and the director alignment profile across the channel with different controlling parameters. Before exploring the effects of the individual parameters, we note few general important characteristics of the director distribution. We observe a periodic pattern of the director alignment, the amplitude of which varies with different flow conditions. It is further seen that the director distortion at the surface is small and remains close to the homeotropic alignment, a result consistent with the assumption for inclusion of the second-order elasticity. The aspect of antisymmetry with the director alignment [39] has also been captured. With these general considerations, we proceed to reflect on the influence of individual parameters on the director distortion. In Fig. 2(a) we show the effect of second-order elasticity effect by imposing a high value of the dimensionless Rapini-Papoular anchoring energy constant ($\bar{\gamma}$). It is intuitive to think that under such strong anchoring the boundary-wise director alignment will follow the exact homeotropic case. Contrary to that, the surface elasticity reduces the effective surface anchoring energy strength [46,47] and causes the boundary alignment to differ from the ideal homeotropic one. This can be comprehended by observing Eqs. (16) and (17), where simply putting $K^* = 0$ will reduce the usual strong boundary conditions, while the mixed splay-bend elastic constant K_{13} becomes redundant. However, accounting for nonvanishing K^* modifies the anchoring energy since K_{13} effectively destabilizes the pre-imposed homogeneous planar orientation. Figure 2(b) depicts the second-order elasticity effect in the presence of sufficiently weak dimensionless Rapini-Papoular anchoring constant ($\bar{\gamma} = 1$). Comparing Figs. 2(a) and 2(b), it is evident that the second-order elasticity effect increases significantly when the dimensionless Rapini-Papoular anchoring energy constant ($\bar{\gamma}$) is reduced. Hence, it confirms the coupling between the effects induced by the parameters b and $\bar{\gamma}$. In both the figures, we compared the distortion behavior of the second-order elasticity theory, which is adopted here, and the conventional Oseen-Frank elasticity theory of first order.

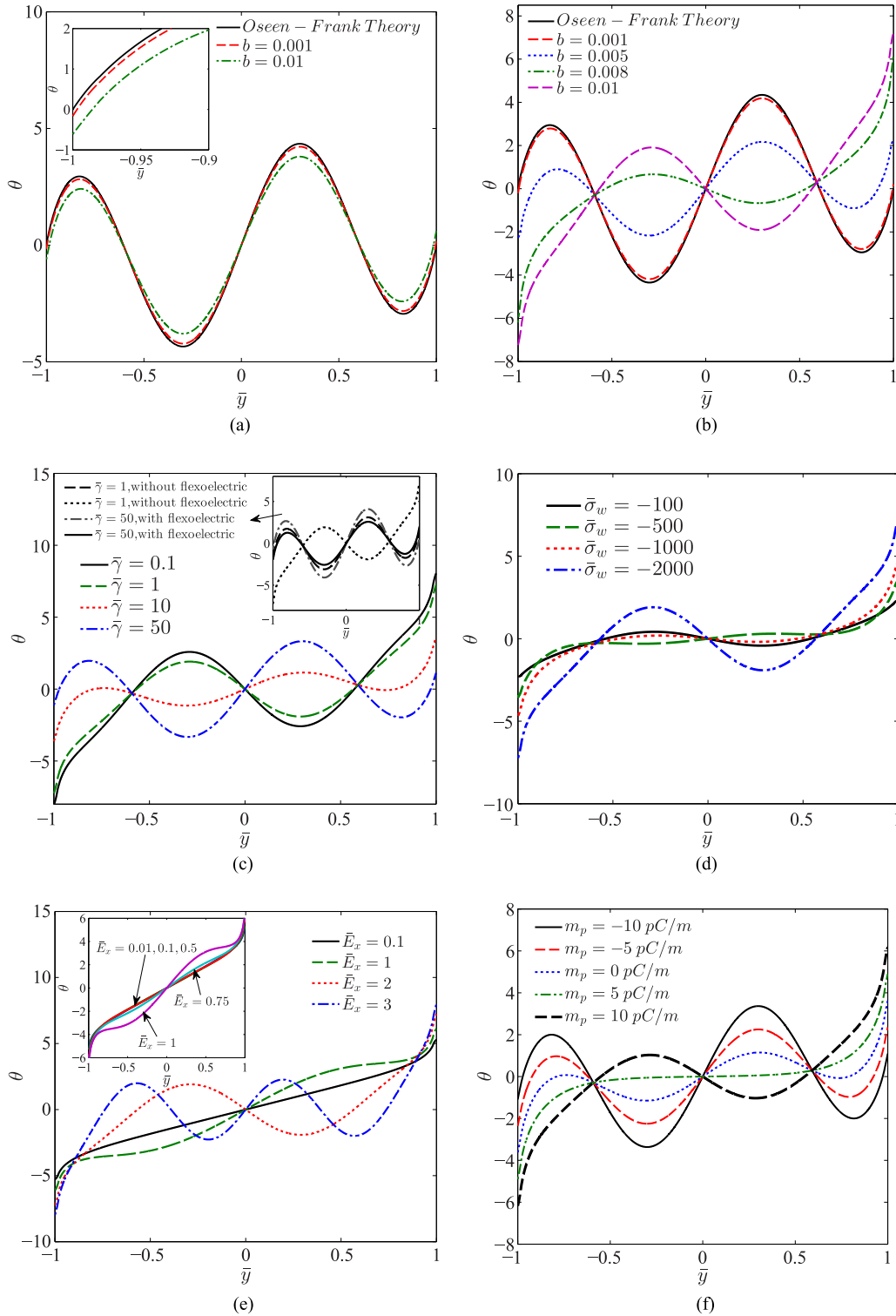


FIG. 2. The variation of the director alignment profile θ as a function of the channel transverse direction \bar{y} for different values of (a) dimensionless second-order elastic constant with strong anchoring, (b) second-order elastic constant with weak anchoring ($\bar{\gamma} = 1$), (c) dimensionless surface anchoring strength, (d) dimensionless surface charge density, (e) dimensionless axial applied field \bar{E}_x and (f) surface polarization (for $\bar{\gamma} = 10$).

From Fig. 2(b), it is observed that with increased second-order elastic coefficient, there occurs a sharper surface distortion of the director. Consideration of Oseen–Frank first-order elasticity theory with only the Rapini–Papoular anchoring

energy in the boundary conditions does not capture the sharp distortion behavior close to the boundaries, while the present considerations shows increase in sharp variations with increase in second-order elastic constant parameter b . These

characteristic director orientations confined near the surface depletion region lead to a varied director configuration across the channel, which implicitly reflects the impact of the surface phenomena into the bulk. Figure 2(c) depicts the effect of the surface anchoring strength on the director alignment. It is clearly evident that as the anchoring energy constant $\bar{\gamma}$ is enhanced, the boundary asymptotically exhibits a strong anchoring behavior, thereby imposing the easy axis alignment on the director at the boundaries, which in our case is the homeotropic alignment ($\theta \rightarrow 0$). It is also counterintuitive to observe that the anchoring constant $\bar{\gamma}$, though it appears in the mathematical equations only through the boundary conditions, shows an evident effect on the bulk director distortion behavior. This can be again substantiated by the comparable channel thickness (~ 1 to $10 \mu\text{m}$) and the extrapolation length ($L_{ex} = K_{11}/W_S \sim 0.12 - 6 \mu\text{m}$) for the present study. In the inset of the same figure, we depicted the influence of flexoelectricity on the nematic director distortion subjected to different $\bar{\gamma}$. Taking into account the flexoelectric contribution in surface free energy causes a reduction in effective anchoring energy [98], and hence, we observe larger distortions along the boundaries. The flexo-induced deformations are generally observed to increase with decreasing anchoring energy constant. Similar trends have been noticed in Fig. 2(c) where the flexo-induced deformations are seen to be more pronounced at low values of $\bar{\gamma}$.

Figure 2(d) depicts the director configuration across the channel for different values of induced surface charge density. The induced charge has an intrinsic effect on the director deformation at the surface, due to a coupled effect of the transverse electric field-induced aligning and flow-induced aligning. With an increase in surface charge, the transverse field tends to orient the director in homeotropic alignment while the increased flow [as seen in Fig. 4(b)] tends to shift such orientation, resulting in the configuration as seen above. Figure 2(e) describes the director configuration for different values of the applied axial electric field \bar{E}_x . It is seen that as the applied field is increased, the director tries to orient itself along the field near the boundaries, thus deviating further from the perfect homeotropic limit. Also, with higher applied field, the frequency of the periodic configuration of the director increases. Such a periodic configuration has been experimentally observed in nonlinear Electro-osmosis flow of NLCs [15]. In the inset of Fig. 2(e), it is shown that the application of an applied axial field (\bar{E}_x) will only influence the equilibrium director configuration if (\bar{E}_x) crosses a threshold value ($\bar{E}_x \geq \bar{E}_{x,c}$). Till this threshold value of the electric field is reached (e.g., $\bar{E}_{x,c} \sim 0.7$ for the presented case), the directors assume a configuration corresponding to the nonflow condition. This phenomenon has a resemblance to the so-called *Fredericksz Transition*, widely introduced in LC literatures [13]. Such a transition from aperiodic to periodic director distribution has been observed in different physical situations where an external magnetic or electric field is applied in nematic cells [99–103]. In Fig. 2(f), we elaborate the effect of surface polarization on the director configuration. We have carefully chosen values of the surface dipole density m_p to remain consistent with the assumption of small subsurface deformation angle. The figure shows that the distortion along the boundaries is significantly affected by the increasing value

of $|m_p|$. While the increasing positive values of $|m_p|$ try to deviate the surface tilt away from the easy axis, its negative values stabilize the distortions more toward the easy axis, which is homeotropic under the present consideration. This behavior is consistent with previous studies [75,76] where the influence of surface polarization effectively alters the apparent flexoelectric effect. The same can be mathematically visualized by having a closer look at the boundary conditions [Eq. (27)] containing the term $(e_3 - m_p)$.

It is worthy to mention here that the oscillating patterns observed are not occurring solely due to the second-order elasticity or weak anchoring boundary condition. Rather, the physical conditions of the problem give rise to such patterns even in the cases of first-order elasticity and strong anchoring strength [please refer to Figs. 2(a) and 2(b)]. A critical observation of the above figures pertaining to the periodic nature of the distortion behavior reveals that the wavelength of a distortion depends strongly on the applied electric field while the other physical mechanisms, such as boundary charging, nonuniform induced electrostatic field, second-order elasticity, anchoring strength, flexoelectricity, and surface polarization have hardly any effect on the same. Contrary to that, the amplitude of such oscillations are dominated by different physical parameters, including the applied electric field. The physical origin of such oscillating patterns can be described as follows. Under application of an electric field beyond a critical value the equilibrium gets destabilized. Due to the inherent tendency of the liquid crystal molecules they try to reorient themselves so as to achieve lowest free energy. The physical conditions of the present problem suggest that the director distortion behavior depends on the anisotropic viscous and elastic properties of the nematic medium. The competitive nature of viscous drag, elastic, and electric forces dictates the optimal wavelength of such periodic distortion [99]. The oscillatory profile of the director at certain values of external electric field as well as the dependence of such oscillation amplitudes and frequencies have been widely observed in a variety of experimental conditions pertaining to nematic liquid crystals [104–106].

Figure 3 illustrates the dimensionless equilibrium electrostatic potential distribution due to the induced EDL across the channel section. Due to the assumption of induced negative charge at the substrate surfaces, a potential distribution with negative sign is observed. The resultant induced field not only affects the flow but also influences the director configuration, which, in turn, affects the flow rheology. In Fig. 3(a), we note the variation of the potential distribution for different values of the induced surface charge density. Higher surface charge implies a higher potential magnitude, and thereby, a stronger transverse electric field. A stronger electric field implies that the field attempts to orient the director along its direction, besides inducing a higher body force for the flow actuation. A coupled effect results in the director configuration as observed in Fig. 2(c). The surface potential, however, does not linearly increase with the surface charge as seen in the inset. This leads to a nonlinear variation of the flow velocity with increase in $\bar{\sigma}_w$.

Figure 3(b) relates the potential distribution for different values of the dimensionless Debye length $\bar{\lambda}$. The factor $\bar{\lambda}$ signifies the apparent penetration of Debye length into the

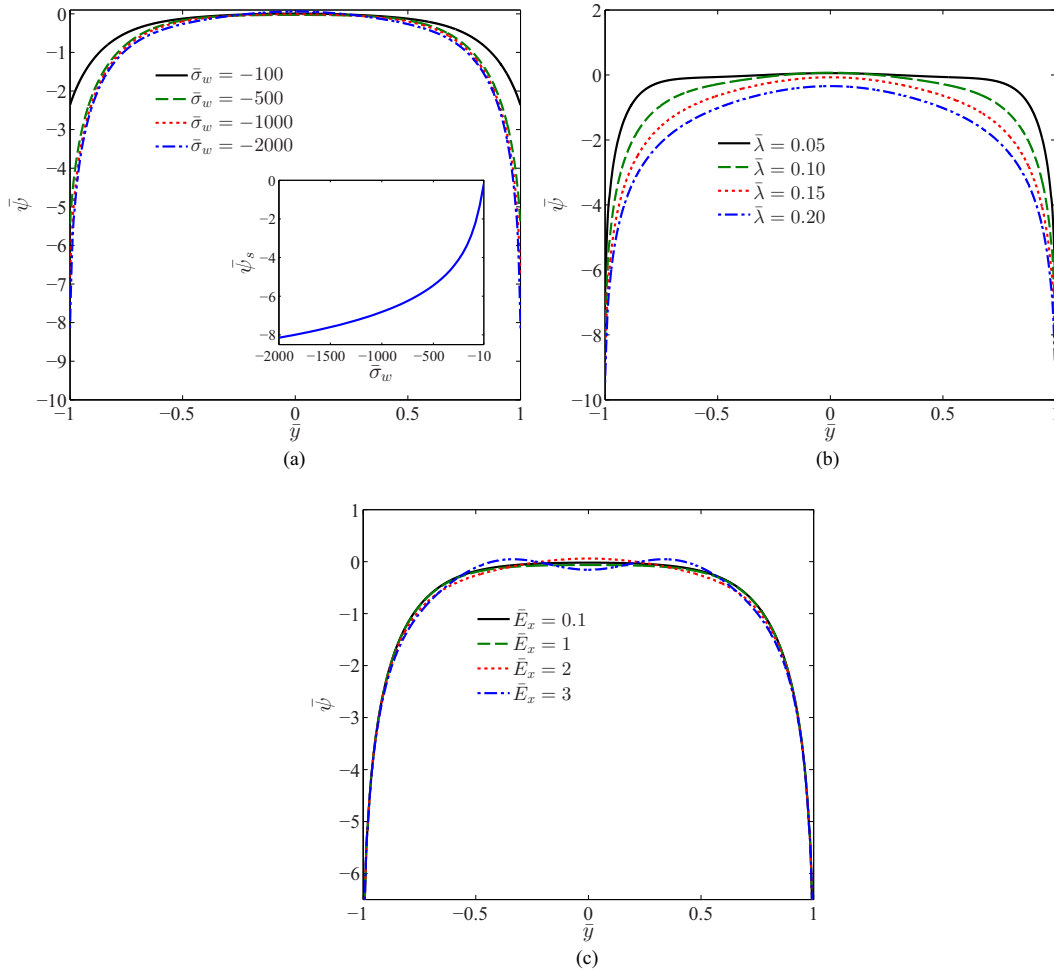


FIG. 3. Variation of the potential distribution $\bar{\psi}$ as a function of the channel transverse direction \bar{y} for different values of dimensionless (a) surface charge density, (b) Debye length, and (c) axial applied field \bar{E}_x .

channel centerline. Consequently, the electrical double layer and the induced transverse field dominate across a larger span of the channel, the result of which is manifested in a larger

flow velocity as will be seen later. Figure 3(c) illustrates the potential distribution variation across the channel due to the applied electric field. It must be noted here that for steady

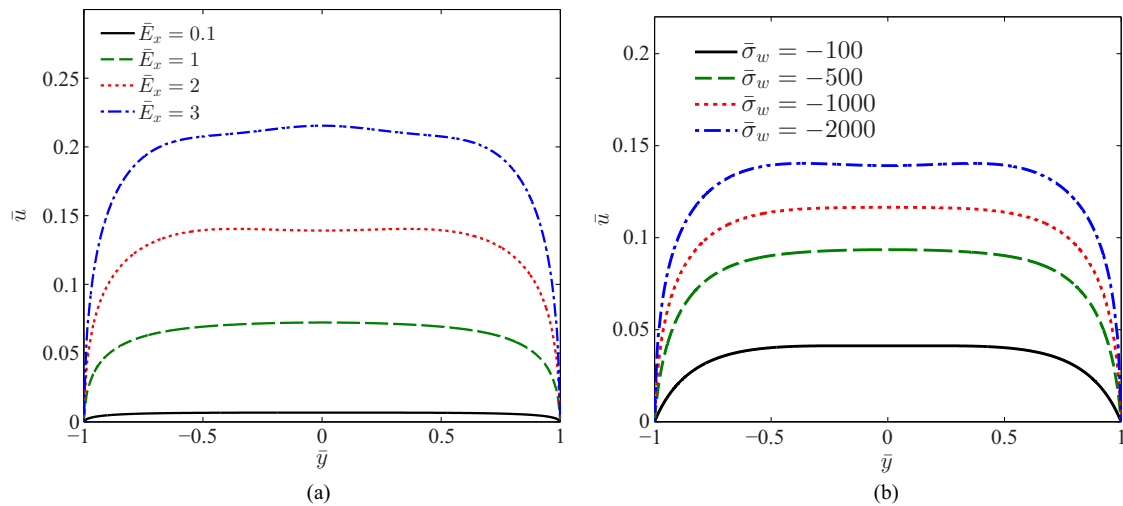


FIG. 4. Variation of the velocity field profile \bar{u} as a function of the channel transverse direction \bar{y} for different values of dimensionless (a) axial applied field \bar{E}_x and (b) surface charge density $\bar{\sigma}_w$.

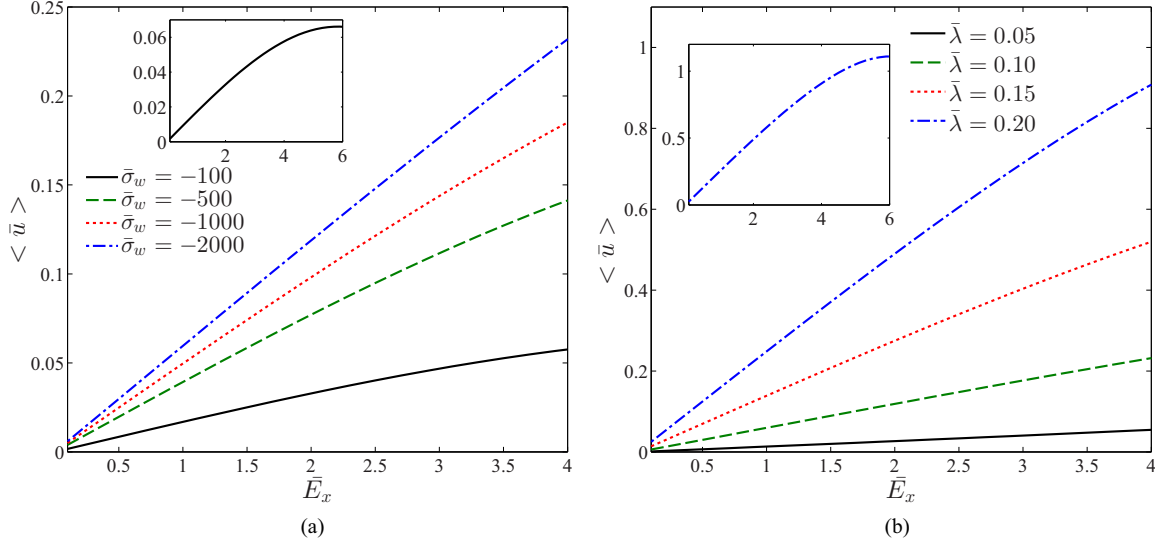


FIG. 5. Variation of the average velocity as a function of the axial field \bar{E}_x for different values of the (a) dimensionless surface charge density and (b) dimensionless Debye screening length $\bar{\lambda}$.

unidirectional electro-osmotic flows of aqueous electrolyte through slit geometries, the potential distribution remains unaffected by the applied axial field. However, for NLC medium, the field has a direct effect on the director distribution, which intrinsically modifies the potential distribution across the channel. This coupling of field-dominated director configuration and charge distribution is clearly manifested especially for higher electric fields, as evident from Fig. 3(c).

Figure 4 illustrates the velocity profile characteristics of electro-osmotic flow in NLC fluids for different values of (a) axial field \bar{E}_x and (b) surface charge density $\bar{\sigma}_w$. In both cases, the velocity profile, in similarity with electro-osmotic flows for Newtonian fluids, follows a region of high velocity gradient near the wall and an apparent plug region at the bulk. With an increase in either the axial field or the surface charge density, the flow velocity gets augmented. This is directly accredited to the enhanced electro-osmotic body force due to a rise in either the actuating field or the induced surface charge. The velocity profile for an electro-osmotic flow of liquid crystals experiences drastic variations, depending on various factors related to surface anchoring, genesis of EDL, and the mode of electro-osmotic flow.

In the reported literature, it has been experimentally observed that application of an external electrical field in the nematic phase results in spatial charge separation owing to nonuniform director configuration [11,15]. The interaction of these induced free charges in the bulk with the applied field, in turn, drives a flow where the velocity profile depicts regions of opposite flow patterns [57]. Such flow actuation mechanism belongs to the category of nonlinear electro-osmotic flow. However, in sharp contrast to the above situation, we consider the generation of EDL at the fluid-substrate interface is independent of the applied field. Further, with the consideration of weak anchoring condition at the boundaries, the sharp changes in the director configuration remain suppressed, which translates into a velocity profile similar to that of electro-osmosis in Newtonian medium. It must nevertheless be appreciated that with higher applied field, the amplitude of

the periodic pattern of the director alignment, which is also observed in nonlinear electro-osmotic flows, gets enhanced and induces slight characteristic undulations in the resulting velocity profile. Such undulation pattern in the velocity field gets further augmented with stronger anchoring strength or strong anchoring condition.

Figure 5 depicts the average flow velocity $\langle \bar{u} \rangle$ for the electro-osmosis of NLC for different values of $\bar{\sigma}_w$ and $\bar{\lambda}$. A direct conclusion from the average flow velocity variation clearly suggests the flow characteristics belong to linear electro-osmosis system, wherein the velocity varies linearly with the electric field, until a critical value of the external field is reached. However, beyond a particular strength of the applied field, a nonlinear behavior is observed. This may be directly attributed to the director deformation due to the applied field. Stronger director deformation leads to anisotropic permittivity-governed charge separation, which is only a function of the applied field [29]. This leads to the variation of the velocity profile from the classical plug-like flow. It is, thus, interesting to observe the effect of parameters such as dimensionless surface charge density ($\bar{\sigma}_w$) and the dimensionless Debye screening length ($\bar{\lambda}$) on the linear to nonlinear transition of the average velocity profiles with external electric field. Owing to the positive dielectric anisotropy of 5CB molecules, increase in $\bar{\sigma}_w$ will try to hold.

Figure 5(a) illustrates that the average velocity gradually increases with an increase in the surface charge density. This is attributed to the corresponding increase of the transverse field with higher surface charge that enhances the effective flow body force, and thereby, the flow average velocity. It is further seen that at higher surface charge density, the linear electro-osmotic regime extends till a higher field compared to lower surface charge densities. At higher surface charge, larger potential due to EDL is generated compared to the charge-separation potential generated due to the applied field attributed to the anisotropic permittivity, and hence, the flow is primarily governed by electrokinetic effects depicting a linear regime. However, at larger fields or lower surface charge

densities, the charge separation potential is comparable to EDL potential and the nonlinear effects creep in. Figure 5(b) also shows that the dimensionless average velocity magnitude increases with increase in $\bar{\lambda}$. However, it must be noted that the reference velocity also increases with $\bar{\lambda}$, according to the method of nondimensionalization framework followed. As a result, the corresponding dimensional velocity is less as EDL thickens ($\bar{\lambda}$ increases). This may directly be explained from the fact that thinner EDL provides stronger electro-osmotic force, and hence, larger average velocity is encountered. We also observe that for thin EDLs (lower values of $\bar{\lambda}$), the linear regime is encountered even at higher applied fields. This contribution comes from the fact that at thin EDL limit, the linear electro-osmotic body force is much stronger compared to the forces generated due to permittivity anisotropic-driven charge separation. Hence, the linear electro-osmosis effect remains predominant in comparison to the cases of thicker EDLs.

Hence, as one increases the applied field, the nonlinear response of the average velocity to the applied field becomes prominent. However, we must strongly note that our nematodynamic formalism developed here is valid for lower applied field strengths where the director deformations are small. The assumption of small director deformation is employed to linearize the second-order elastic equations near the boundary. At large applied fields, the director deformation becomes large, which renders this assumption invalid, and thereby, our formulation will not hold physical meaning. Further, as mentioned earlier, very high values of external electric field and/or other controllable dimensionless parameters may result in increasingly higher flow velocities and the corresponding Ericksen number will increase accordingly, making the flow more prone towards the development of topological defects. Thus, we have restricted our study to the analysis of NLC electro-osmosis within the domain of linear dynamics.

IV. CONCLUSIONS

Here, we have studied electro-osmotically actuated flows of complex NLC fluids through microconfinement with surface-dominated characteristics. Governing formulation of the problem is devised based on fundamental free-energy considerations, taking into account the intricate anisotropic dielectric and viscous features of the NLC medium. The nematic-substrate interaction has been characterized by weak anchoring, surface elasticity coupled with second-order elastic constant. Due to proper characterization of such surface influences, second-order elastic theory and weak anchor-

ing energies have been considered to model the director configuration with the assumption of small deformations near the surface. The flexoelectric polarization and surface polarization are taken into account to accurately model such interaction. In contrast to the induced charge electro-osmosis recently studied in nematics liquid crystal [57], triggered due to imposed director patterning, here we have focused on the classical electrokinetics based on the selective ion adsorption at the surface. The EDL is modeled with a modified Poisson-Boltzmann equation considering excluded volume effects, while the equations are closed with the LE theory governing the electro-osmotic flow velocity profile. The important observations from the present study are:

1. Application of electric field beyond a critical value induces periodic oscillations in the director field. The amplitude of such periodic behavior depends on most of the physical variables, while the wavelength is dictated by the external field only.

2. The oscillating nature of the flow velocity and electrostatic potential was captured. The coupling of director orientation with the nonuniform electrostatic potential and flow velocity becomes prominent, especially through the prominent oscillating behavior of the same. This observation is quite specific to the NLC medium considered, contrary to the steady electro-osmotic flows of aqueous electrolytes, where the potential distribution gets unaffected by the applied axial field.

3. The parameters characterizing the nematic-substrate interaction show their dominance by modifying the effective surface anchoring strength. Due to comparable dimension of narrow confinement under consideration and the extrapolation length of anchoring strength, the surface effects penetrate far into the bulk distortion behavior.

4. The flexoelectric polarization shows its effect both in surface and volume torque balances, and thus, play a prominent role in modifying the effective anchoring strength as well as the fluctuating nature of the director distortion. The flexoeffects are found to be more prominent at sufficiently weak Rapini-Papoular anchoring energy strength.

Importantly, we observe that the average velocity increases linearly with the electric field, indicating the flow to be in purview of linear electro-osmosis. Here we must note that the LE formulation used above satisfactorily captures experimental observations investigated previously. The current analysis, thus, stands as a precursor to further experimental studies in regard to linear electro-osmosis, which gives an opportunity to devise intriguing flow control by modulation of surface patterning, applied field, and intrinsic characteristics of NLC medium.

[1] S. Chakraborty, *Anal. Chim. Acta* **605**, 175 (2007).
 [2] A. Bandopadhyay, U. Ghosh, and S. Chakraborty, *J. Nonnewton. Fluid Mech.* **202**, 1 (2013).
 [3] J. Dhar, A. Bandopadhyay, and S. Chakraborty, *Phys. Rev. E* **88**, 053001 (2013).
 [4] S. K. Sia and G. M. Whitesides, *Electrophoresis* **24**, 3563 (2003).

[5] D. J. Beebe, G. A. Mensing, and G. M. Walker, *Annu. Rev. Biomed. Eng.* **4**, 261 (2002).
 [6] S. Das, T. Das, and S. Chakraborty, *Sensors Actuators B Chem.* **114**, 957 (2006).
 [7] F. H. J. Van Der Heyden, D. J. Bonthuis, D. Stein, C. Meyer, and C. Dekker, *Nano Lett.* **7**, 1022 (2007).

- [8] F. H. J. van der Heyden, D. J. Bonthuis, D. Stein, C. Meyer, and C. Dekker, *Nano Lett.* **6**, 2232 (2006).
- [9] A. Bandopadhyay and S. Chakraborty, *Langmuir* **27**, 12243 (2011).
- [10] S. Das and S. Chakraborty, *Langmuir* **26**, 11589 (2010).
- [11] I. Lazo, C. Peng, J. Xiang, S. V. Shiyankovskii, and O. D. Lavrentovich, *Nat. Commun.* **5**, 5033 (2014).
- [12] P. G. de Gennes and J. Prost, *The Physics of Liquid Crystals*, 2nd ed. (Clarendon Press, Oxford, 1993).
- [13] I. W. W. Stewart, *The Static and Dynamic Continuum Theory of Liquid Crystals* (Taylor and Francis, London/New York, 2004).
- [14] A. Sengupta, S. Herminghaus, and C. Bahr, *Liq. Cryst. Rev.* **2**, 37 (2014).
- [15] C. Peng, Y. Guo, C. Conklin, J. Viñals, S. V. Shiyankovskii, Q.-H. Wei, and O. D. Lavrentovich, *Phys. Rev. E* **92**, 052502 (2015).
- [16] S. Shi and H. Yokoyama, *Langmuir* **31**, 4429 (2015).
- [17] A. Sengupta, *Liq. Cryst. Today* **24**, 70 (2015).
- [18] R. J. Hunter, *Zeta Potential in Colloid Science. Principles and Applications* (Academic Press, New York, 1981).
- [19] J. H. Masliyah and S. Bhattacharjee, *Electrokinetic and Colloid Transport Phenomena* (John Wiley & Sons, Inc., Hoboken, NJ, 2006).
- [20] D. Chakraborty and S. Chakraborty, in *Microfluidics and Microfabrication*, edited by S. Chakraborty (Springer U.S., Boston, MA, 2010), pp. 1–85.
- [21] S. Talapatra and S. Chakraborty, *Eur. J. Mech. B/Fluids* **27**, 297 (2008).
- [22] S. Chakraborty and A. K. Srivastava, *Langmuir* **23**, 12421 (2007).
- [23] D. Pal and S. Chakraborty, *Electrophoresis* **32**, 638 (2011).
- [24] J. J. Bikerman, *Z. Phys. Chem. A* **163**, 378 (1933).
- [25] S. Chakraborty and S. Ray, *Phys. Fluids* **20**, 083602 (2008).
- [26] M. Z. Bazant and T. M. Squires, *Curr. Opin. Colloid Interface Sci.* **15**, 203 (2010).
- [27] T. M. Squires and M. Z. Bazant, *J. Fluid Mech.* **509**, 217 (2004).
- [28] J. A. Levitan, S. Devasenathipathy, V. Studer, Y. Ben, T. Thorsen, T. M. Squires, and M. Z. Bazant, *Colloids Surf. A Physicochem. Eng. Asp.* **267**, 122 (2005).
- [29] O. M. Tovkach, M. C. Calderer, D. Golovaty, O. Lavrentovich, and N. J. Walkington, *Phys. Rev. E* **94**, 012702 (2016).
- [30] O. D. Lavrentovich and V. M. Pergamenschchik, *Phys. Rev. Lett.* **73**, 979 (1994).
- [31] H. Yokoyama, *Mol. Cryst. Liq. Cryst. Inc. Nonlin. Opt.* **165**, 265 (1988).
- [32] S. A. Jewell, S. L. Cornford, F. Yang, P. S. Cann, and J. R. Sambles, *Phys. Rev. E* **80**, 041706 (2009).
- [33] L. M. Blinov, A. Y. Kabayenkova, and A. A. Sonin, *Liq. Cryst.* **5**, 645 (1989).
- [34] K. Ichimura, T. Seki, A. Hosokita, and K. Aoki, *Langmuir* **4**, 1214 (1988).
- [35] J. P. Bramble, S. D. Evans, J. R. Henderson, C. Anquetil, D. J. Cleaver, and N. J. Smith, *Liq. Cryst.* **34**, 1059 (2007).
- [36] V. K. Gupta, *Science* **276**, 1533 (1997).
- [37] E. Mema, L. Kondic, and L. J. Cummings, *Phys. Rev. E* **95**, 012701 (2017).
- [38] A. Rapini and M. Papoular, *J. Phys. Colloq.* **30**, C4-54 (1969).
- [39] G. Barbero, N. V. Madhusudana, and C. Oldano, *J. Phys. France* **50**, 2263 (1989).
- [40] G. Barbero and C. Oldano, *Mol. Cryst. Liq. Cryst. Inc. Nonlin. Opt.* **170**, 99 (1989).
- [41] J. Nehring and A. Saupe, *J. Chem. Phys.* **54**, 337 (1971).
- [42] J. Nehring, *J. Chem. Phys.* **56**, 5527 (1972).
- [43] I. Lelidis and G. Barbero, *Liq. Cryst.* **43**, 208 (2016).
- [44] S. Stallinga and G. Vertogen, *Phys. Rev. E* **53**, 1692 (1996).
- [45] P. Guyot-Sionnest, H. Hsiung, and Y. R. Shen, *Phys. Rev. Lett.* **57**, 2963 (1986).
- [46] G. Barbero and A. Strigazzi, *Liq. Cryst.* **5**, 693 (1989).
- [47] S. Faetti, *Liq. Cryst.* **15**, 807 (1993).
- [48] S. Faetti, *Phys. Rev. E* **49**, 5332 (1994).
- [49] S. Faetti, *Mol. Cryst. Liq. Cryst. Sci. Technol. Sect. A. Mol. Cryst. Liq. Cryst.* **241**, 131 (1994).
- [50] G. Barbero and G. Durand, *J. Phys. France* **51**, 281 (1990).
- [51] G. Barbero and G. Durand, *J. Appl. Phys.* **67**, 2678 (1990).
- [52] R. R. Shah and N. L. Abbott, *J. Phys. Chem. B* **105**, 4936 (2001).
- [53] A. V. Zakharov and R. Y. Dong, *Phys. Rev. E* **65**, 052701 (2002).
- [54] K. Kočevar and I. Mušević, *Phys. Rev. E* **65**, 030703(R) (2002).
- [55] L. A. T. Espinoza, K. R. Schumann, Y. Y. Luk, B. A. Israel, and N. L. Abbott, *Langmuir* **20**, 2375 (2004).
- [56] M. C. Calderer, D. Golovaty, O. Lavrentovich, and N. J. Walkington, *SIAM J. Appl. Math.* **76**, 2260 (2016).
- [57] C. Conklin and J. Viñals, *Soft Matter* **13**, 725 (2017).
- [58] M. S. Kilic, M. Z. Bazant, and A. Ajdari, *Phys. Rev. E* **75**, 021502 (2007).
- [59] R. N. Thurston, J. Cheng, R. B. Meyer, and G. D. Boyd, *J. Appl. Phys.* **56**, 263 (1984).
- [60] R. N. Thurston, *J. Appl. Phys.* **55**, 4154 (1984).
- [61] S. Chandrasekhar, *Liquid Crystals*, 2nd ed. (Cambridge University Press, Cambridge, 1992).
- [62] M. Buczkowska, *Liq. Cryst.* **37**, 1331 (2010).
- [63] G. Derfel and M. Buczkowska, *Liq. Cryst.* **40**, 272 (2013).
- [64] M. Buczkowska and G. Derfel, *Liq. Cryst.* **41**, 169 (2014).
- [65] G. Derfel and M. Buczkowska, *Liq. Cryst.* **42**, 1213 (2015).
- [66] H. J. Deuling, *Mol. Cryst. Liq. Cryst.* **19**, 123 (1972).
- [67] V. M. Pergamenschchik, P. I. C. Teixeira, and T. J. Sluckin, *Phys. Rev. E* **48**, 1265 (1993).
- [68] S. Stallinga, J. A. M. M. van Haaren, and J. M. A. van den Eerenbeemd, *Phys. Rev. E* **53**, 1701 (1996).
- [69] I. Dahl and A. De Meyere, *Liq. Cryst.* **18**, 683 (1995).
- [70] S. Faetti, *Phys. Rev. E* **49**, 4192 (1994).
- [71] G. Arfken, *Mathematical Methods for Physicists*, 2nd ed. (Academic Press, San Diego, 1973).
- [72] G. Barbero, A. Sparavigna, and A. Strigazzi, *Nuovo Cim. D* **12**, 1259 (1990).
- [73] N. É. Ágnes Buka, *Flexoelectricity in Liquid Crystals Theory, Experiments and Applications* (Imperial College Press, London, 2013).
- [74] D.-K. Yang and S.-T. Wu, *Fundamentals of Liquid Crystal Devices* (John Wiley & Sons, Ltd, Chichester, UK, 2014).
- [75] A. Derzhanski, A. G. Petrov, and M. D. Mitov, *J. Phys. France* **39**, 273 (1978).
- [76] A. G. Petrov and A. Derzhanski, *Mol. Cryst. Liq. Cryst.* **41**, 41 (1977).
- [77] V. G. Nazarenko, R. Klouda, and O. D. Lavrentovich, *Phys. Rev. E* **57**, R36 (1998).
- [78] G. Barbero, L. R. Evangelista, and N. V. Madhusudana, *Eur. Phys. J. B* **1**, 327 (1998).

- [79] M. Monkade, P. Martinot-Lagarde, and G. Durand, *Europhys. Lett.* **2**, 299 (1986).
- [80] S. Majumder, J. Dhar, and S. Chakraborty, *Sci. Rep.* **5**, 14725 (2015).
- [81] M. Z. Bazant, B. D. Storey, and A. A. Kornyshev, *Phys. Rev. Lett.* **106**, 046102 (2011).
- [82] D. Ben-Yaakov, D. Andelman, D. Harries, and R. Podgornik, *J. Phys. Condens. Matter* **21**, 424106 (2009).
- [83] S. Das, A. Guha, and S. K. Mitra, *Anal. Chim. Acta* **804**, 159 (2013).
- [84] G. Chen and S. Das, *J. Colloid Interface Sci.* **445**, 357 (2015).
- [85] V. Freedericksz and V. Zolina, *Trans. Faraday Soc.* **29**, 919 (1933).
- [86] A. V. Zakharov and R. Y. Dong, *Phys. Rev. E* **64**, 042701 (2001).
- [87] G. Barbero and C. Oldano, *Mol. Cryst. Liq. Cryst. Inc. Nonlin. Opt.* **168**, 1 (1989).
- [88] D. S. Seo, H. Matsuda, T. Oh-ide, and S. Kobayashi, *Mol. Cryst. Liq. Cryst. Sci. Technol. Sect. A. Mol. Cryst. Liq. Cryst.* **224**, 13 (1993).
- [89] Y. Yi, G. Lombardo, N. Ashby, R. Barberi, J. E. Maclennan, and N. A. Clark, *Phys. Rev. E* **79**, 041701 (2009).
- [90] H. Yokoyama and H. A. Van Sprang, *J. Appl. Phys.* **57**, 4520 (1985).
- [91] A. Sengupta, B. Schulz, E. Ouskova, and C. Bahr, *Microfluid. Nanofluidics* **13**, 941 (2012).
- [92] C. Zhou, P. Yue, and J. J. Feng, *J. Fluid Mech.* **593**, 385 (2007).
- [93] C. Liu and M. C. Calderer, *SIAM J. Appl. Math.* **60**, 1925 (2000).
- [94] M. C. Calderer and B. Mukherjee, *Liq. Cryst.* **22**, 121 (1997).
- [95] M. C. Calderer, *Eur. J. Appl. Math.* **8**, 301 (1997).
- [96] A. V. Zakharov and R. Y. Dong, *Eur. Phys. J. E* **6**, 3 (2001).
- [97] L. M. Blinov, M. I. Barnik, H. Ohoka, M. Ozaki, N. M. Shtykov, and K. Yoshino, *Eur. Phys. J. E* **4**, 183 (2001).
- [98] D. Olivero, L. R. Evangelista, and G. Barbero, *Phys. Rev. E* **65**, 031721 (2002).
- [99] G. Srajer, S. Fraden, and R. B. Meyer, *Phys. Rev. A* **39**, 4828 (1989).
- [100] E. Miraldi, C. Oldano, and A. Strigazzi, *Phys. Rev. A* **34**, 4348 (1986).
- [101] E. Bodenschatz, W. Zimmermann, and L. Kramer, *J. Phys. France* **49**, 1875 (1988).
- [102] A. J. Hurd, S. Fraden, F. Lonberg, and R. B. Meyer, *J. Phys. France* **46**, 905 (1985).
- [103] F. Lonberg and R. B. Meyer, *Phys. Rev. Lett.* **55**, 718 (1985).
- [104] W. Greubel and U. Wolff, *Appl. Phys. Lett.* **19**, 213 (1971).
- [105] B. H. Soffer, J. D. Margerum, A. M. Lackner, D. Boswell, A. R. Tanguay, T. C. Strand, A. A. Sawchuk, and P. Chavel, *Mol. Cryst. Liq. Cryst.* **70**, 145 (1981).
- [106] J. M. Pollack and J. B. Flannery, in *Liquid Crystal Ordered Fluids*, edited by J. F. Johnson and R. S. Porter (Springer U.S., Boston, MA, 1974), pp. 557–571.